Electronic Supplementary Material (ESI) for ChemComm.

Supplementary Material for

Multifaceted magnetization dynamics in the mononuclear complex $[Re^{IV}Cl_4(CN)_2]^{2-}$

Xiaowen Feng,[a] Jun-Liang Liu,[b,c,d] Kasper S. Pedersen,[c,d,e] Joscha Nehrkorn,[f] Alexander Schnegg,[f] Karsten Holldack,[g] Jesper Bendix,[h] Marc Sigrist,[i,j] Hannu Mutka,[i] Dumitru Samohvalov,[c,d] David Aguilà,[c,d] Ming-Liang Tong,[b] Jeffrey R. Long[a,k,l,*] and Rodolphe Clérac,[c,d,*]

[a] Department of Chemistry, University of California Berkeley, California, 94720, USA.
[b] MOE Key Lab of Bioinorganic and Synthetic Chemistry, State Key Laboratory of Optoelectronic Materials and Technologies, School of Chemistry & Chemical Engineering, Sun Yat-sen University, Guangzhou 510275, P. R. China.
[c] CNRS, CRPP, UPR 8641, F-33600 Pessac, France.
[d] Univ. Bordeaux, CRPP, UPR 8641, F-33600 Pessac, France.
[e] CNRS, ICMCB UPR 9048, 33608 Pessac Cedex, France.
[f] Helmholtz-Zentrum für Materialien und Energie, Institut für Silizium-Photovoltaik, 12489 Berlin, Germany.
[g] Helmholtz-Zentrum für Materialien und Energie, Inst. f. Methoden und Instrumente der Forschung mit Synchrotronstrahlung, 12489 Berlin, Germany.
[h] Department of Chemistry, University of Copenhagen, DK-2100 Copenhagen, Denmark.
[i] Institut Laue-Langevin, 38042 Grenoble Cedex 9, France.
[j] Institute of Chemistry, Academia Sinica, Nankang, 11529 Taipei, Taiwan, ROC.
[k.] Materials Sciences Division, Lawrence Berkeley National Laboratory, Berkeley, California 94720, USA.
[l.] Department of Chemical and Biomolecular Engineering, University of California Berkeley, Berkeley, California 94720, USA.

Correspondence to: clerac@crpp-bordeaux.cnrs.fr, jrlong@berkeley.edu

Table of Contents

Materials and Methods

1.1 Synthesis of $(Bu_4N)_2[Re^{IV}Cl_4(CN)_2]\cdot 2DMA$ (1). The synthesis of $(Bu_4N)_2[Re^{IV}Cl_4(CN)_2]\cdot 2DMA$ was performed following previously reported method.[1] 0.4 g solid $(Bu_4N)CN$ was added to a stirred green solution of *cis*-$[ReCl_4(THF)_2]$ (0.2 g) in 2 mL of DMF under nitrogen. The resulting dark brown solution was allowed to stir overnight and then exposed to air. Addition of 25 mL of water to the solution resulted in the formation of a brown precipitate. The precipitate was collected after filtration, washed with water and diethyl ether, and allowed to dry under vacuum for 1 hour. The pale brown solid was then dissolved in 1.5 mL of *N*,*N*-dimethylacetamide (DMA), and the resulting dark yellow solution was filtered through diatomaceous earth. Diffusion of diethyl ether vapor into the resulting filtrate yielded pale blue rod-shaped crystals suitable for X-ray diffraction. Anal. Calcd for $C_{42}H_{90}N_6Cl_4O_2Re$: C, 48.54; N: 8.09; H: 8.73. Found: C, 48.49; N: 8.07; H: 8.63. IR (300 K): $\overline{\nu}_{CN}$ = 2120 cm^{-1}.

1.2 X-ray crystal structure at 50 K. The crystal structure was collected at the Stanford Nano Shared Facilities (SNSF). Single crystal of $(Bu_4N)_2[Re^{IV}Cl_4(CN)_2]\cdot 2DMA$ (1) was coated with Paratone-N oil and mounted on glass fibers. The crystal was then quickly transferred to a Bruker D8 Venture diffractometer, and cooled cooled to 50 K using Helium with an N-HeliX from Oxford Cryosystems. Space group assignments were based upon systematic absences, E-statistics, and successful refinement of the structure. Structure was solved by direct methods and expanded through successive difference Fourier maps. They were refined against all data using the SHELXTL[2] program. Thermal parameters for all non-hydrogen atoms were refined anisotropically.

1.3 Magnetic Measurements. The magnetic measurements were carried out with the use of Quantum Design MPMS-XL SQUID magnetometer and PPMS-9 susceptometer. These instruments work between 1.8 and 400 K with applied dc fields ranging from -7 to 7 T (MPMS). Measurements were performed on a polycrystalline samples of **1** sealed in a polyethylene bag ($3 \times 0.5 \times 0.02$ cm; typical 20 to 40 mg) and covered with mineral oil or directly in their frozen mother liquor within a sealed straw to prevent desolvation of the solid. No evaporation of the mother liquor was observed during these measurements. The mass of the sample was determined after the measurements and subsequent mother liquor evaporation. Prior to the experiments, the field-dependent magnetization was measured at 100 K in order to confirm the absence of any bulk ferromagnetic impurities. Ac susceptibility measurements were made with an oscillating field of 1 to 6 Oe with a frequency from 10 to 10000 Hz (PPMS). The magnetic data were corrected for the sample holder, mineral oil, mother liquor and the intrinsic diamagnetic contributions.

1.4 Other Physical Measurements. Infrared spectra were obtained on a Perkin-Elmer Spectrum 400 FTIR spectrometer equipped with an attenuated total reflectance (ATR) accessory. Carbon, hydrogen, and nitrogen analyses were obtained from the Microanalytical Laboratory of the University of California, Berkeley.

1.5 Inelastic Neutron Scattering. INS spectra of polycrystalline **1** were obtained by the direct geometry, time-of-flight spectrometer IN5 at the Institut Laue-Langevin, Grenoble, France. Approximately 0.5 g of a nondeuterated polycrystalline sample was loaded into a 10-mm-diameter double-wall hollow aluminum cylinder. A standard ILL

Orange cryostat was employed. The data were reduced and analyzed using the LAMP program package.[3]

1.6 Frequency-domain Fourier-transform THz-EPR. FD-FT THz-EPR experiments were performed at the THz beamline at the BESSY II storage ring. The setup employing coherent synchrotron radiation is described in detail elsewhere.[4,5] In short, coherent synchrotron radiation[6] with strong intensity in the THz range is coupled out from the synchrotron, and passed through an FT-IR spectrometer. After passing a polarization retarder the radiation is focused on the sample placed in an optical magnet. The transmitted intensity is detected by a Si-bolometer immersed in superfluid Helium. **1** was investigated as polycrystalline powder frozen in the solvent and also as 76 mg finely ground powder mixed with 100 mg polyethylene and pressed to a pellet (weight 161 mg). In the following we will abbreviate them as polycrystalline and pellet sample, respectively. Experimental resolution was 0.5 cm^{-1}. These FT-IR based experiments required a reference. As the undamped synchrotron radiation would completely saturate the detector we could not use an empty magnet or a polyethylene pellet as reference. Therefore we used spectra of the sample measured at elevated temperatures as reference. Hence the transmission is obtained by dividing the spectra measured at low temperature by that measured at the elevated temperature which was for all the experiments at 33 K. Recently, it was found that it is often useful to divide spectra measured at different magnetic fields but the same low temperature.[5,7,8] In this way non-magnetic transmission changes are canceled out.

References

1. T. D. Harris, M. V. Bennett, R. Clérac, J. R. Long, *J. Am. Chem. Soc.* 2010, **132**, 3980.
2. G. M. Sheldrick, SHELXTL, Version 6.12; Bruker Analytical X-Ray Systems, Madison, WI, 2000.
3. D. Richard, M. Ferrand, G. J. Kearley, *J. Neutron Res.* 1996, **4**, 33.
4. A. Schnegg, J. Behrends, K. Lips, R. Bittl, K. Holldack, *Phys. Chem. Chem. Phys.* 2009, **11**, 6820.
5. J. Nehrkorn, B. M. Martins, K. Holldack, S. Stoll, H. Dobbek, R. Bittl, A. Schnegg, *Mol. Phys.* 2013, **111**, 2696.
6. Abo-Bakr, M.; Feikes, J.; Holldack, K.; Kuske, P.; Peatman, W. B.; Schade, U.; Wüstefeld, G.; Hübers, H. W. *Phys. Rev. Lett.* **2003**, *90*, 094801.
7. Nehrkorn, J.; Telser, J.; Holldack, K.; Stoll, S.; Schnegg, A. *J. Phys. Chem. B* **2015**, *119*, 13816.
8. Rechkemmer, Y.; Breitgoff, F. D.; van der Meer, M.; Atanasov, M.; Hakl, M.; Orlita, M.; Neugebauer, P.; Neese, F.; Sarkar, B.; van Slageren, J. *Nat Commun* **2016**, *7*.

Table S1. Selected Mean Interatomic Distances (Å) and Angles (°) for **1** at 139 K and 50 K.

	139 K	**50 K**
Re-Cl	2.3509(9), 2.3407(10)	2.3212(15), 2.3357(15)
Re-C	2.148(4)	2.140(5)
Re-C-N	177.2(3)	177.8(5)
Cl-Re-Cl	90.13(4)	90.18(5)
C-Re-Cl	88.58(10), 89.57(10)	88.28(15), 89.92(15)

Table S2. Crystallographic data for **1** at 139 K and 50 K.

	139 K	**50 K**
Crystal system	triclinic	
Space group	*P*-1	
***a* / Å**	10.5629(8)	10.4031(6)
***b* / Å**	11.9119(9)	11.9265(7)
***c* / Å**	12.1271(9)	11.9819(7)
***α* / °**	64.8130(10)	64.8219(16)
***β* / °**	75.0150(10)	75.0617(17)
***γ* / °**	82.1510(10)	82.2082(17)
***V* / Å^3**	1333.2(2)	1299.34(13)
Z	1	
***μ* / mm^{-1}**	2.500	2.581
Refl. Coll. / unique	6616 / 4241	23134 / 6646
R_{int}	0.031	0.086
[a]R_1 ($I > 2\sigma(I)$)	0.0337	0.0624
[b]wR_2 (all data)	0.0859	0.1708
Goodness-of-fit	1.045	1.033
CCDC N°	781037	1488917

[a]$R_1 = \Sigma||F_O|-|F_C||/\Sigma|F_O|$, [b]w$R_2 = [\Sigma w(F_O^2-F_C^2)^2/\Sigma w(F_O^2)^2]^{1/2}$

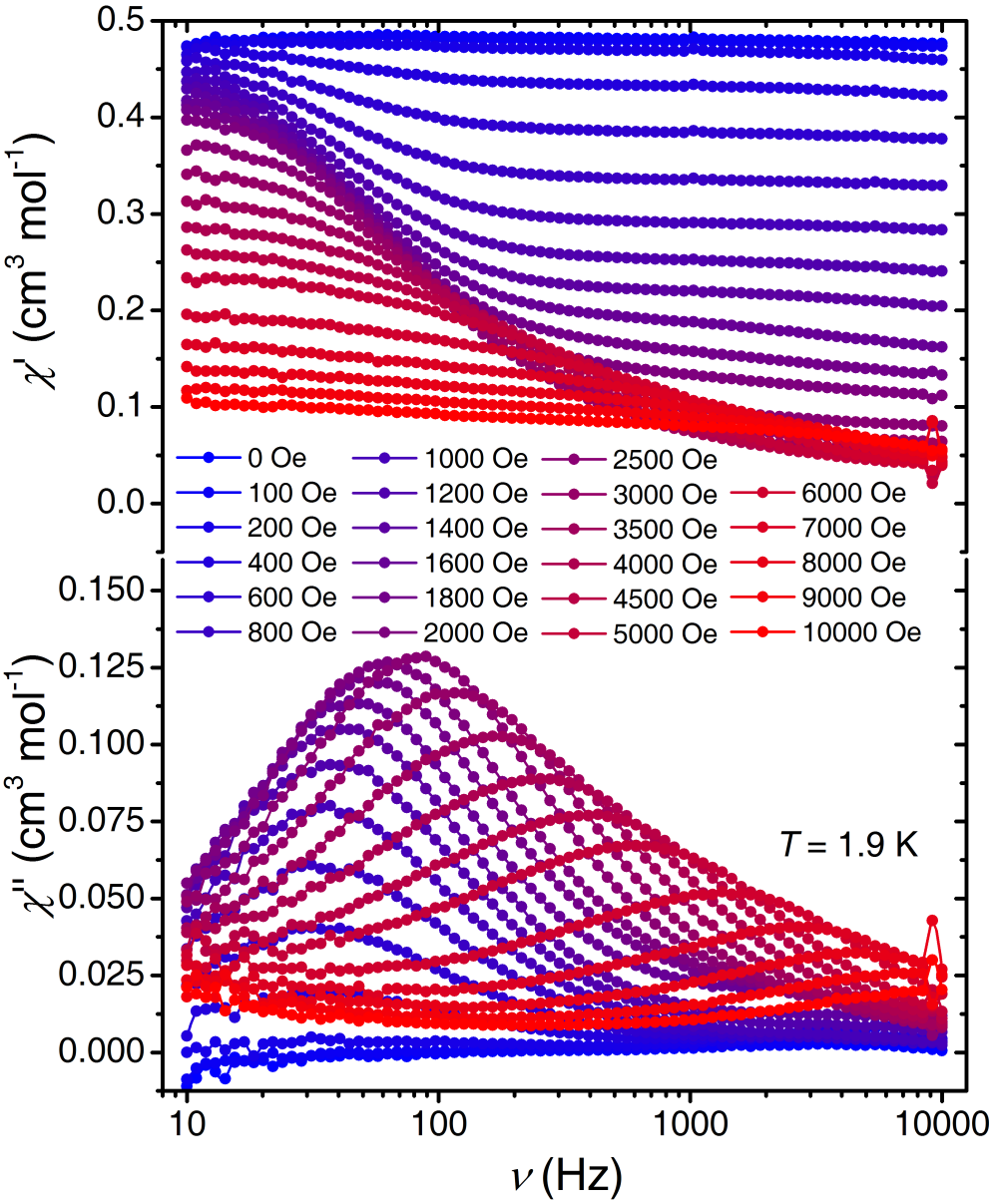

Figure S1. Frequency dependence of the real (χ', top) and imaginary (χ", bottom) parts of the ac susceptibility at 1.9 K under different dc fields for a polycrystalline sample of **1**. Solid lines are guides for the eye.

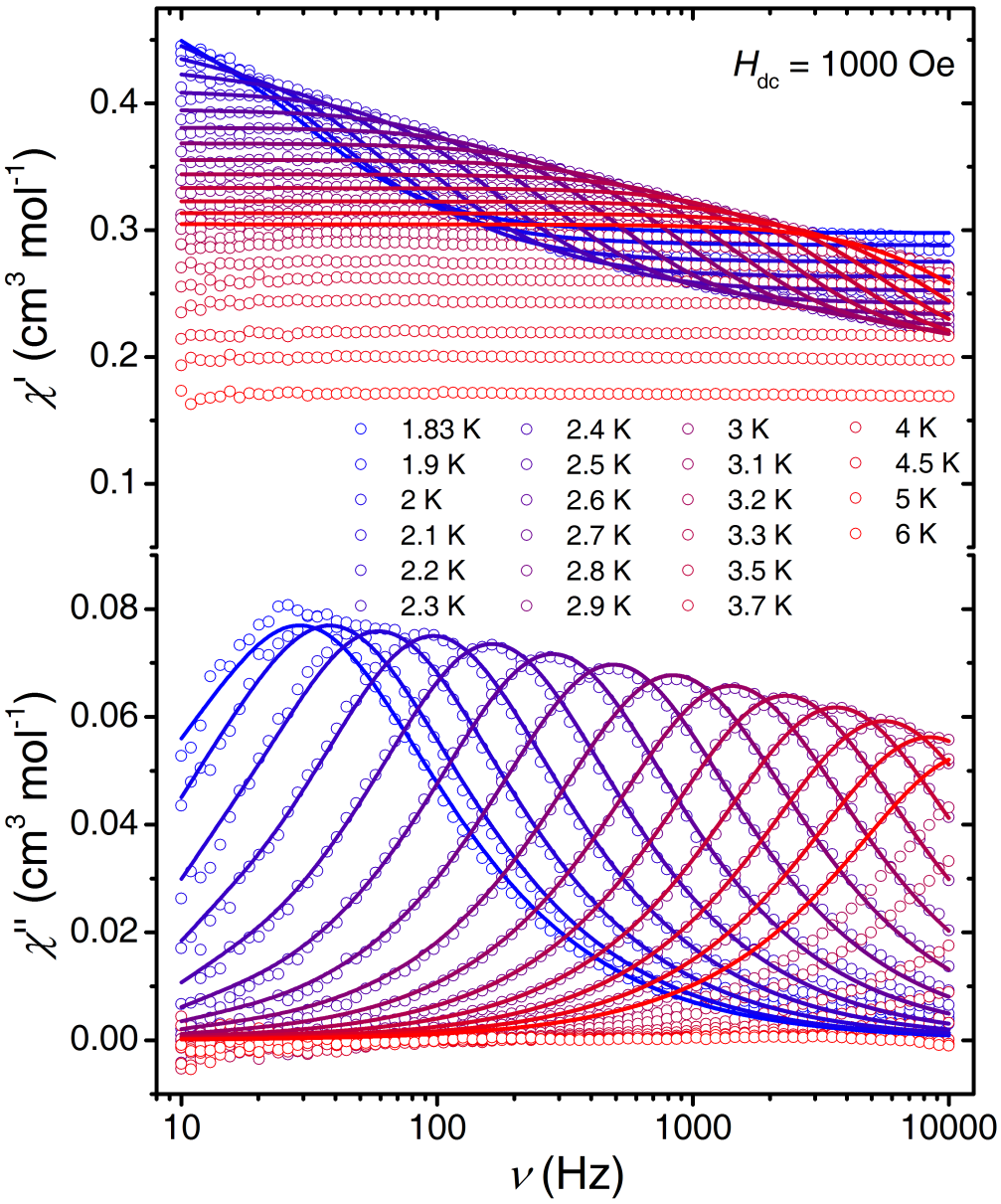

Figure S2. Frequency dependence of the real (χ', top) and imaginary (χ", bottom) parts of the ac susceptibility at different temperatures for a polycrystalline sample of **1** in a 1000 Oe dc field. Solid lines are the best fits for the generalized Debye model.

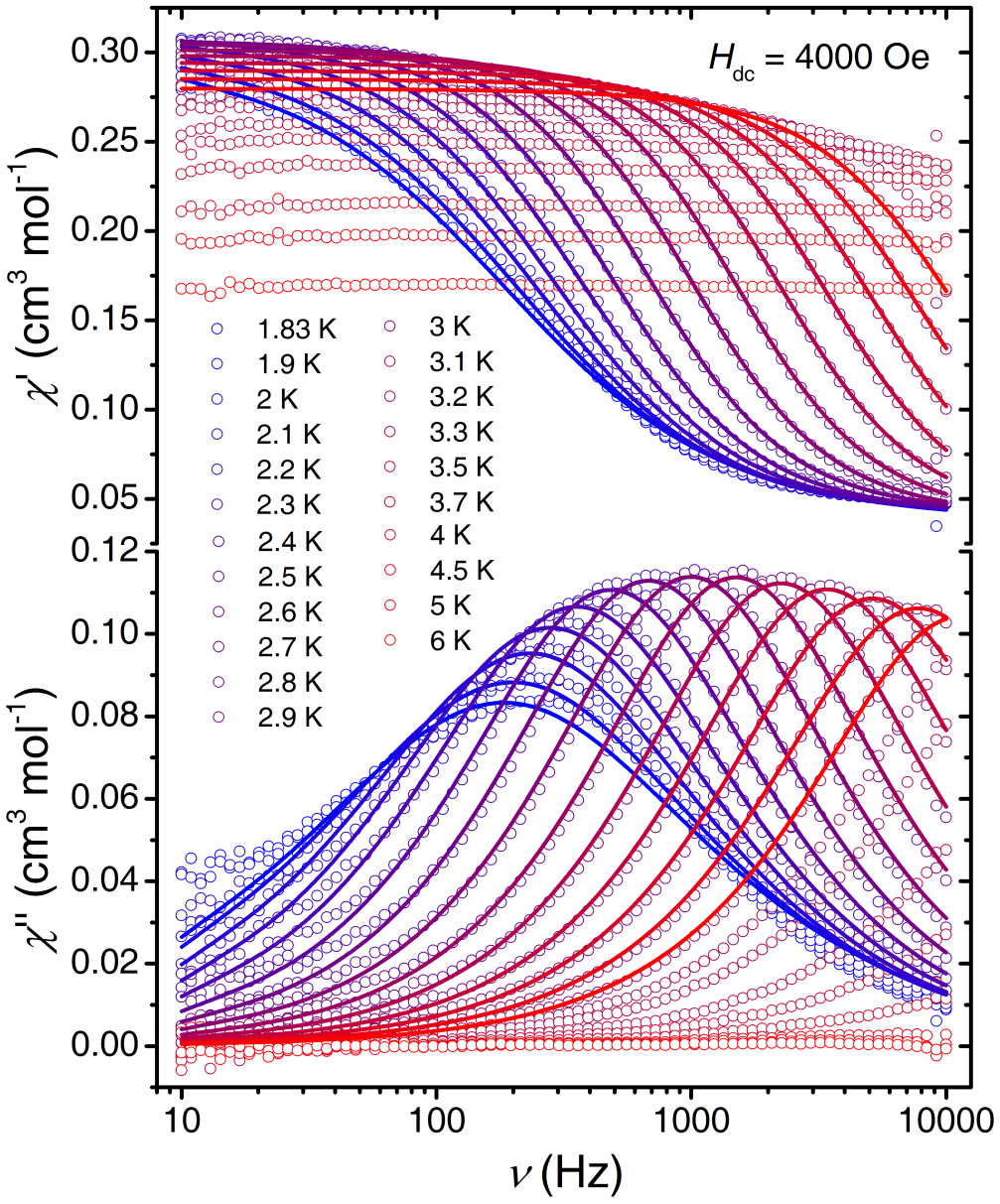

Figure S3. Frequency dependence of the real (χ', top) and imaginary (χ", bottom) parts of the ac susceptibility at different temperatures for a polycrystalline sample of **1** in a 4000 Oe dc field. Solid lines are the best fits for the generalized Debye model.

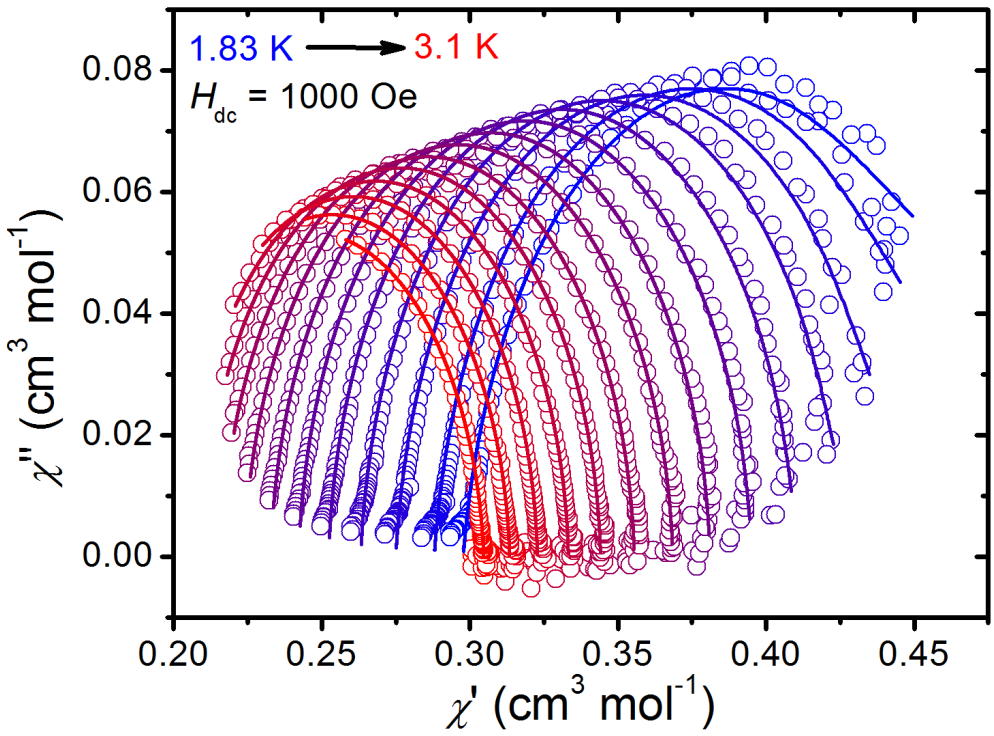

Figure S4. Cole-Cole plots for a polycrystalline sample of **1** at temperatures from 1.83 K to 3.1 K, under 1000 Oe applied dc field. The solid lines correspond to the fits to the data with α values range from 0.03-0.10.

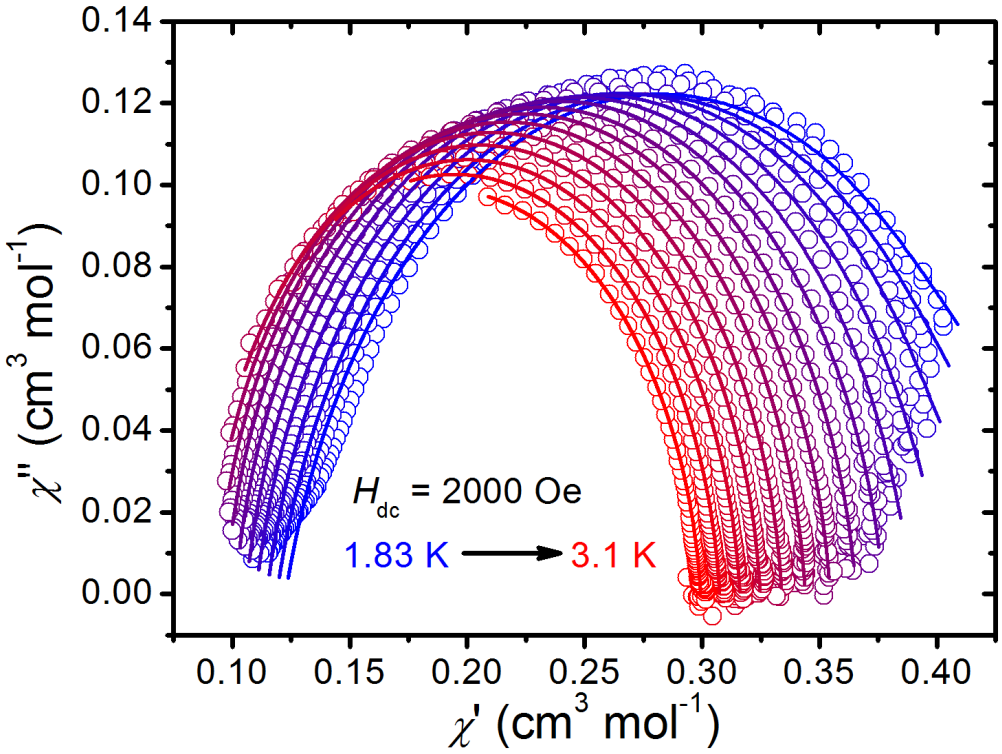

Figure S5. Cole-Cole plots for a polycrystalline sample of **1** at temperatures from 1.83 K to 3.1 K, under 2000 Oe applied dc field. The solid lines correspond to the fits to the data with α values range from 0.03-0.10.

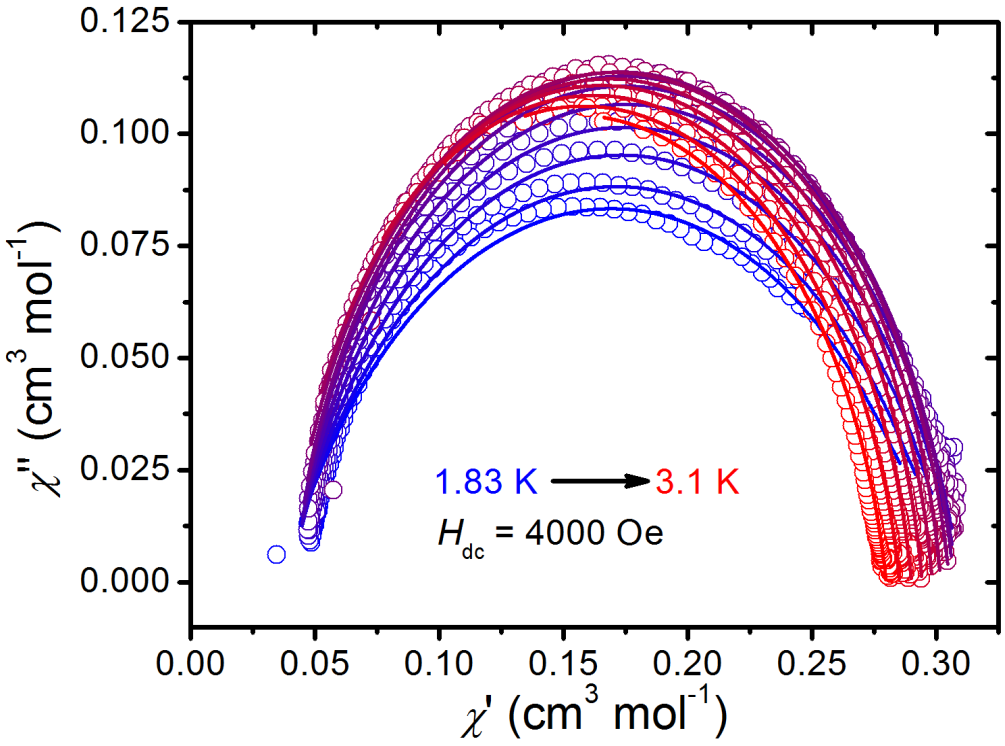

Figure S6. Cole-Cole plots for a polycrystalline sample of **1** at temperatures from 1.83 K to 3.1 K, under 4000 Oe applied dc field. The solid lines correspond to the fits to the data with α values range from 0.03-0.10.

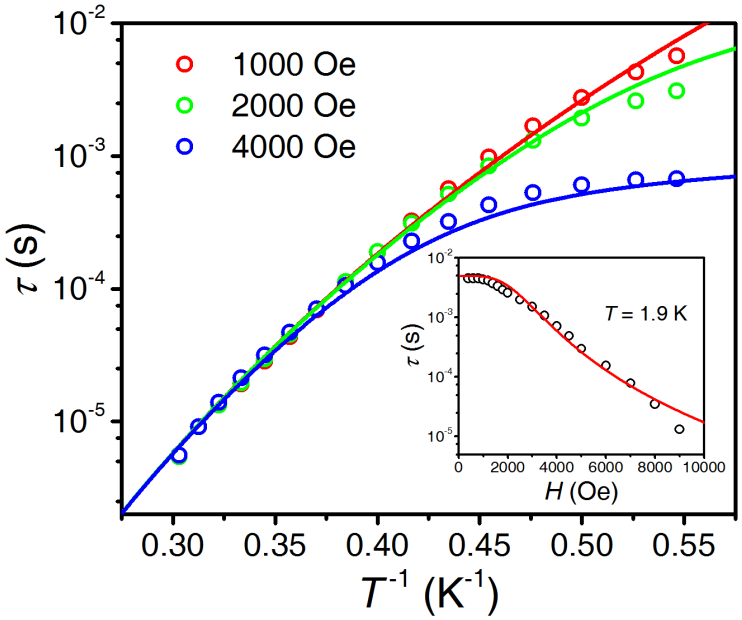

Figure S7. Variable field relaxation time (τ) vs. inverse temperature (T^{-1}). The solid lines are for the fitting model with direct and Raman process which is physically unreasonable based on the large Raman exponent, n = 12 (with A = 3.0×10^{4} s^{-1} K^{-1} T^{-4} (fixed), C = 9.1×10^{-2} s^{-1} K^{-12} and n = 12).

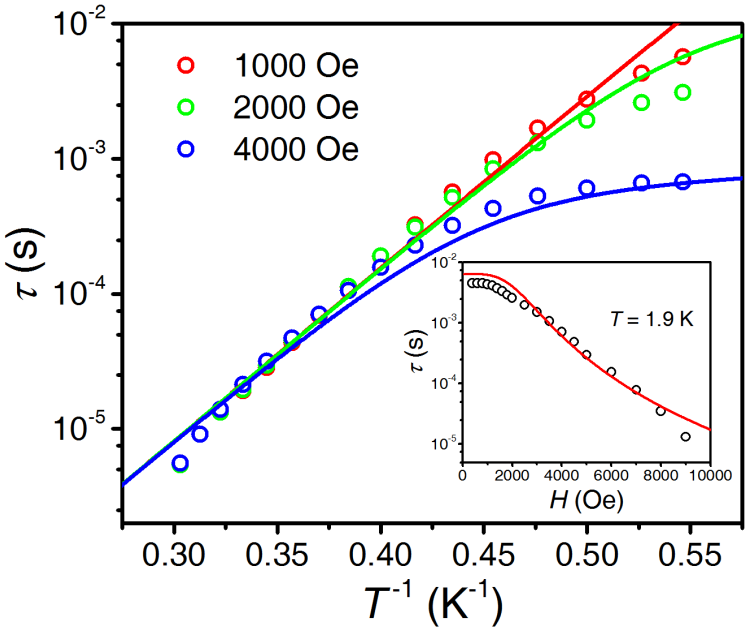

Figure S8. Variable field relaxation time (τ) vs. inverse temperature (T^{-1}). The solid lines are for the fitting model with direct and Orbach processes, which is not fitting well the experimental data (with A = 3.0×10^{4} s^{-1} K^{-1} T^{-4} (fixed), τ_0 = 1.2(4) × 10^{-9} s and Δ_{eff}/k_B = 29 K (20 cm^{-1})).

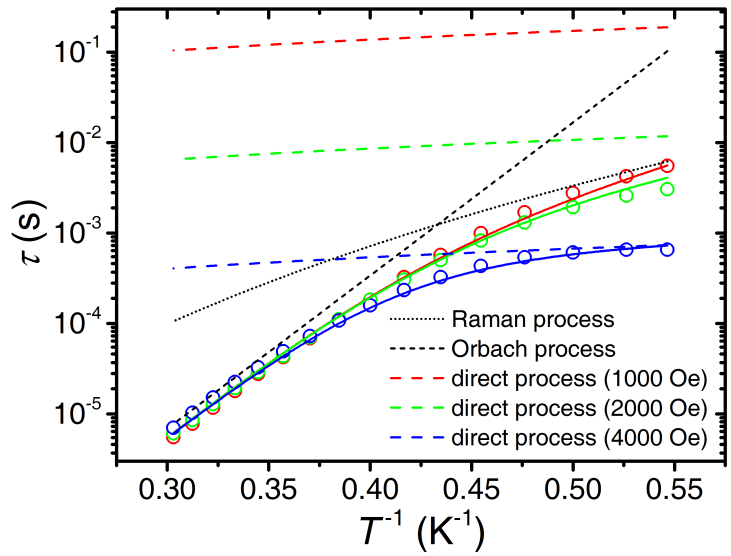

Figure S9. Variable field relaxation time (τ) vs. inverse temperature (T^{-1}). The solid lines are for the eqn 6 fitting model (see main text, Fig. 2) with A = 2.9 × 10^{4} s^{-1} K^{-1} T^{-4}, C = 2.5 s^{-1} $K^{-6.9}$, n = 6.9, τ_0 = 5.7 × 10^{-11} s and Δ_{eff}/k_B = 39 K (27 cm^{-1}). The dotted lines are the contributions of the different relaxation processes as indicated on the legend of the figure.

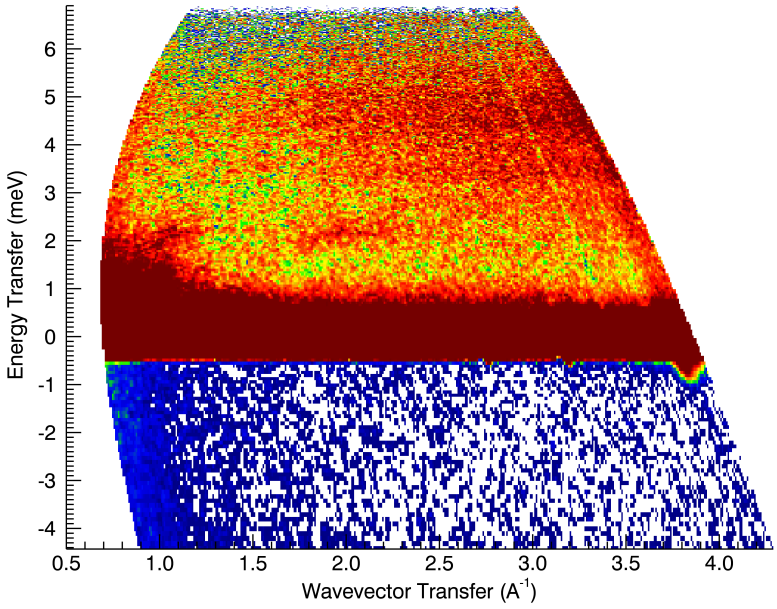

Figure S10. INS spectrum of **1** shown as an intensity *vs.* *Q* (linear momentum) transfer map as obtained at T = 1.5 K and an incident neutron wave length of λ_i = 3.0 Å.

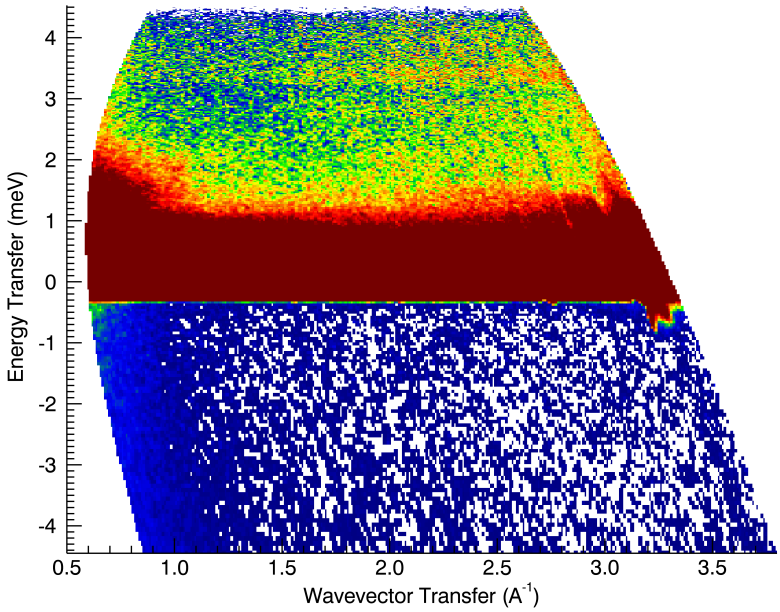

Figure S11. INS spectrum of **1** shown as an intensity *vs. Q* (linear momentum) transfer map as obtained at T = 1.8 K and an incident neutron wave length of λ_i = 3.5 Å.

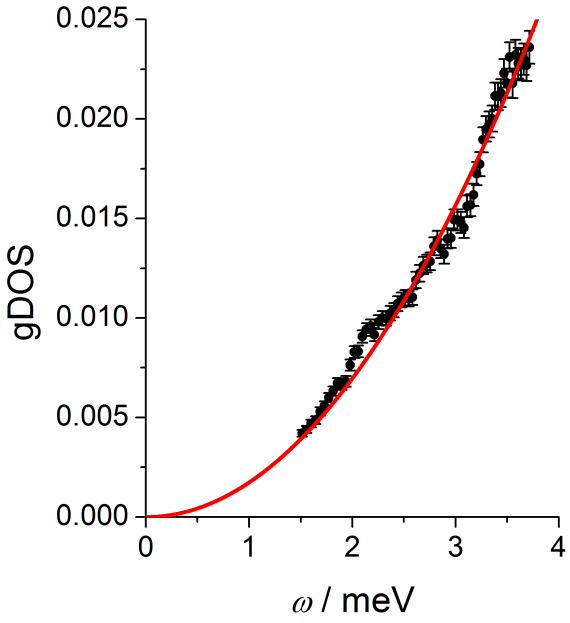

Figure S12. Generalized (neutron) density of states (gDOS) as a function of energy transfer (ω) as extracted from the 3.5 Å INS data (above) following the procedure described by Squires (Introduction to the Theory of Thermal Neutron Scattering, 1997, University of Cambridge, p. 55). The solid red line is the best fit to the function $3\omega^2/\omega_D^3$, where ω_D = 12 meV (139 K) is the Debye energy (temperature).

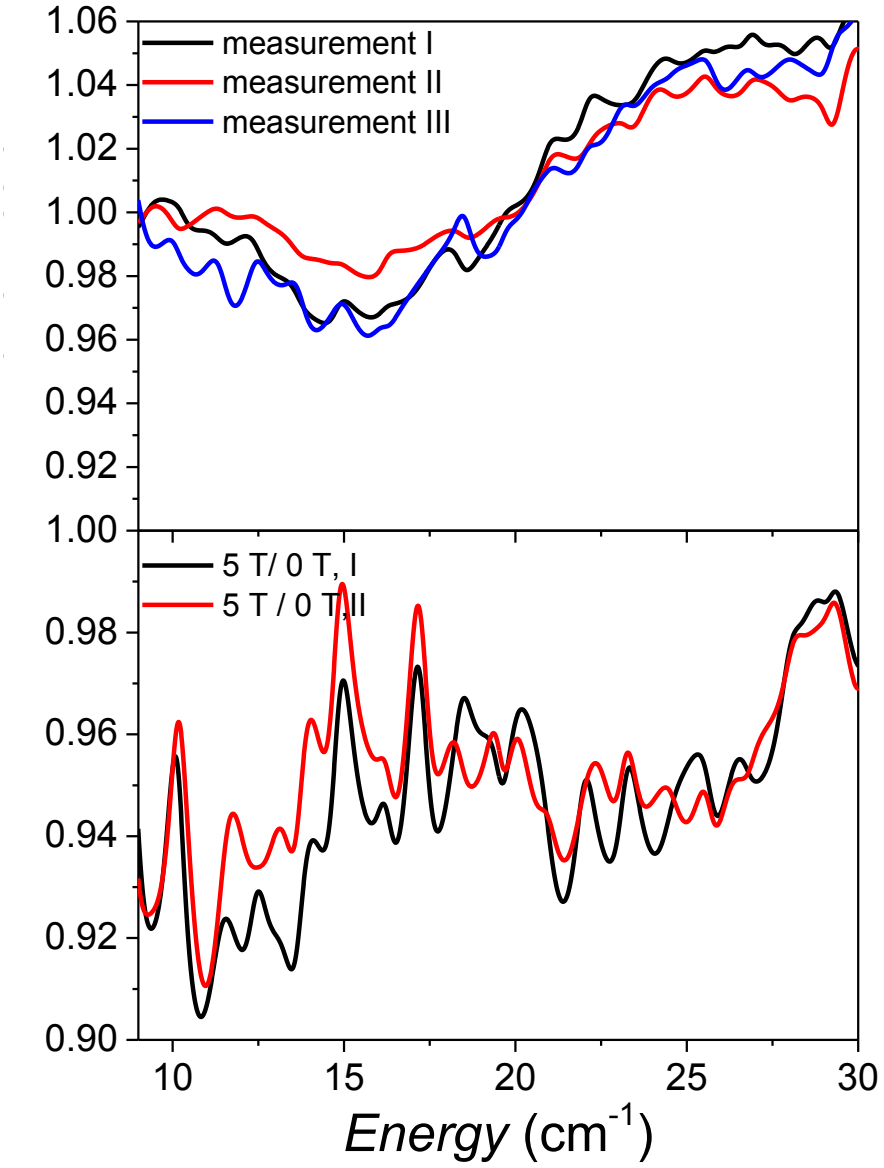

Figure S13. FD-FT THz-EPR spectra of the pellet sample of **1** at *T* = 5 K. The upper panel show transmission in the absence of a magnetic field (reference was a spectrum of the sample measured at 33 K). The measurements were repeated three times under slightly different synchrotron conditions (for each a new reference was also recorded). For energies of 20 cm^{-1} and higher the transmission at 5 K was slightly lower than at 33 K. However no clear feature could be observed. In the bottom panel, spectra measured at 5 K and at fields of 5 and 0 T are divided. The synchrotron radiation decays with time, therefore the measurement order for the two shown spectra is reversed. The observed variations are on the noise level, which was approximately 3% for these experiments. To conclude, no magnetic transition could be observed on the pellet sample of **1** in the spectral range from 8 to 30 cm^{-1} with FD-FT THz-EPR.

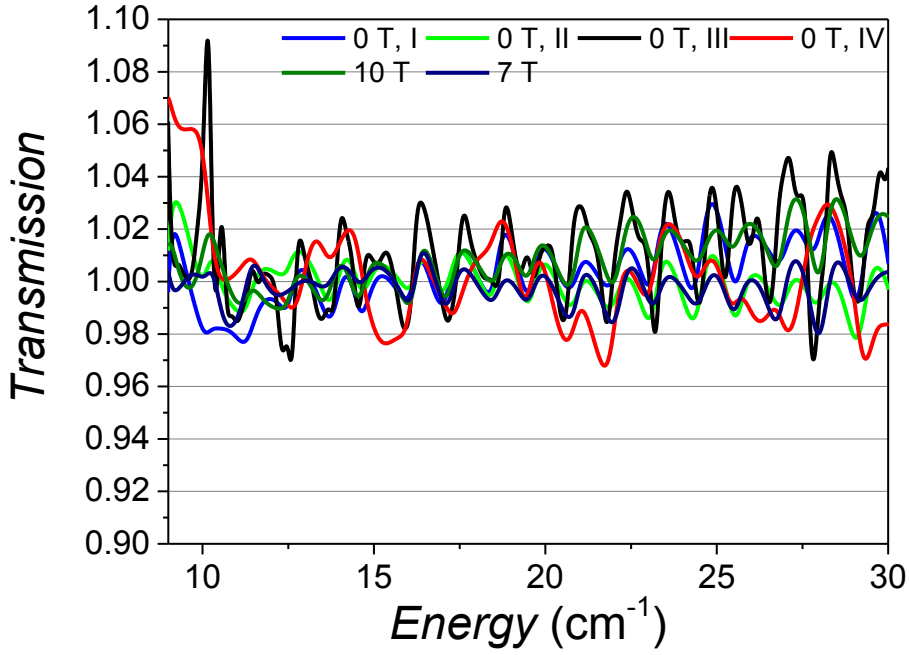

Figure S14. FD-FT THz-EPR spectra of a poly-crystalline sample of **1** at T = 5 K. Reference spectra were measured at the same external magnetic field and at a temperature of 33 K. Transmission was observed as independent of temperature and magnetic field changes in the studied field and temperature range. The variations in the transmission at energies of 10 cm^{-1} and lower are artifacts due to the lower radiation intensity in this spectral range.